ChemPubSoc Europe

DOI: 10.1002/cphc.201201015

3D Nanoscale Chemical Imaging of the Distribution of Aluminum Coordination Environments in Zeolites with Soft X-Ray Microscopy

Luis R. Aramburo,[a] Yijin Liu,[b] Tolek Tyliszczak,[c] Frank M. F. de Groot,[a] Joy C. Andrews,[b] and Bert M. Weckhuysen*[a]

The catalytic and physicochemical properties of zeolite materials are intimately connected with the aluminum content as well as its spatial distribution within the zeolite framework structure.[1–2] Distribution of aluminum and related aluminum zoning can occur at the level of the crystallographic T sites within the zeolite framework structure,[3,4] as well as within a zeolite particle.[5,6] Despite that these are well-known phenomena, further information on aluminum zoning within individual zeolite particles is needed. It is important to recall that the performance of a catalytic material is directly related to the spatial distribution of its active sites,[7–10] which in the case of zeolites, are the Brønsted acid sites, formed by the corner-sharing of aluminum and silicon tetrahedra. The strength of these Brønsted acid sites are therefore directly related to the number and distribution of aluminum atoms in the zeolite particle.[11,12] Furthermore, spatial distribution of aluminum also impacts post-synthetic treatments, such as desilication[13] or steaming,[14] which alter the acidic properties and molecular transport within the zeolite particle.[15–17]

Many characterization methods have been explored to investigate the spatial distribution of aluminum within large micron-sized zeolite crystals and smaller poly-crystalline zeolite aggregates. The techniques include atomic absorption spectrometry (AAS),[18] electron microprobe analysis (EPMA),[19] X-ray fluorescence (XRF),[20] inductively coupled plasma-atomic emission spectroscopy (ICP-AES),[21] fast-atom-bombardment mass spectrometry (FABMS), X-ray photoelectron spectroscopy (XPS),[22] energy-dispersive X-ray spectroscopy (EDX)[23] as well as proton-induced gamma-ray emission (PIGE).[24] Unfortunately, these methods often require sputter or milling pre-treatments to reveal insights from the deeper parts of the zeolite particle. As a consequence, a limited number of the characterization studies report on the distribution of aluminum throughout the entire zeolite particle volume,[25,26] while none of them discriminate between the different coordination environments of aluminum. Within this context, it has been recently shown that 3D scanning transmission X-ray microscopy (STXM) is well suited to chemically probe the interior of micron-sized objects due to a unique combination of the microscope's depth of focus, penetration depth and spatial resolution.[27,28]

Here, we present the first nanoscale chemical imaging study revealing the spatial distribution of the amount and coordination environment of aluminum in zeolite materials with 3D scanning transmission X-ray microscopy (STXM). For this purpose, we have focused on two showcase samples involving the industrially relevant zeolite H-ZSM-5. The first one is a calcined H-ZSM-5 commercial zeolite powder, labeled as ZSM-5-C. The second material with sample name ZSM-5-S has been obtained by steaming ZSM-5-C at 700 °C for 3 h. Further details on the preparation and physicochemical properties of both materials can be found in the Supporting Information of a recent article.[29]

To gain insight into the 3D distribution of the amount of aluminum and its coordination environments within ZSM-5-C and ZSM-5-S, chemical mapping at the aluminum K-edge was done making use of the interferometrically controlled STXM instrument at beamline 11.0.2 of the Advanced Light Source (ALS) of the Lawrence Berkeley National Laboratory (LBNL, Berkeley, USA).[30] 2D STXM images were obtained over 61 different angles (−90°, 90°) with an increment of 3° between each set of images. For this purpose, the zeolite ZSM-5 aggregates were introduced into a glass capillary and positioned perpendicular to the X-ray beam on a tomography sample stage. The set of 2D STXM images was recorded at three different energies, further labeled as E_1, E_2 and E_3, at 1560 eV, 1565.5 eV and 1567 eV, respectively, while the focus settings were optimized at every angle. The STXM images were acquired using a 25 nm Fresnel zone plate, with a spatial resolution set at 30 nm and a field of view of 3×3 μm. Further details concerning the preparation of the glass capillaries, the tomography stage as well as the data-processing routines applied can be found in the Supporting Information.

In order to translate the information within the 2D set of STXM images at different energies and angles in terms of different aluminum coordination environments we have made use of two aluminum reference compounds. The selected com-

[a] L. R. Aramburo,[+] Prof. Dr. F. M. F. de Groot, Prof. Dr. B. M. Weckhuysen
Inorganic Chemistry and Catalysis group
Debye Institute for Nanomaterials Science
Utrecht University, Universiteitsweg 99
3584 CG Utrecht (The Netherlands)
E-mail: b.m.weckhuysen@uu.nl

[b] Dr. Y. Liu,[+] Prof. Dr. J. C. Andrews
Stanford Synchrotron Radiation Lightsource
2575 Sand Hill Road
Menlo Park, California 94025 (USA)

[c] Dr. T. Tyliszczak
Advanced Light Source
Lawrence Berkeley National Laboratory
Berkeley, California 94720 (USA)

[+] Both authors equallly contributed to this work.

Supporting information for this article is available on the WWW under http://dx.doi.org/10.1002/cphc.201201015.

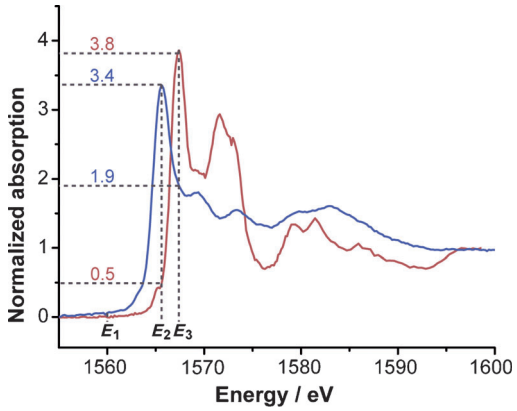

Figure 1. Soft X-ray K-edge absorption spectra of aluminum for reference compounds albite (blue) and corundum (red), including the three energies (E_1, E_2 and E_3) measured at every projection angle during the scanning transmission X-ray microscopy (STXM) tomography measurements. In the case of sample ZSM-5-C E_1, E_2, and E_3 represent the pre-edge feature, the edge jump for 4-fold aluminum and the edge jump for 6-fold aluminum, respectively.

pounds are albite (i.e. a 4-fold aluminum mineral) and corundum (i.e. a 6-fold aluminum mineral). The soft X-ray absorption spectra at the aluminum K-edge of both minerals are given in Figure 1. We have opted for the measurement at three selected energy points E_1, E_2 and E_3 to allow the quantification of 4- and 6-fold aluminum in ZSM-5-C according to the equations given in Scheme SI-1. This quantitative approach applied to each voxel over the entire investigated volume of ZSM-5-C, results in a 3D distribution of the amount of 4- and 6-fold aluminum within the zeolite particle, as shown in Figure 2a. It is important to remark that previous ^{27}Al MAS NMR measurements on ZSM-5-C have shown that this material only contains one type of 4-fold aluminum (87%) with minor amounts of 6-fold coordinated aluminum (13%).[29]

The corresponding movie of the 3D reconstruction of 4- and 6-fold aluminum coordination environments in sample ZSM-5-C is given in Movie SI-1, while Figure 3a shows the 2D STXM slices obtained from the 3D data cube of this movie. These data reveal that an individual ZSM-5-C particle contains a mixture of 4- and 6-fold aluminum species. The 4-fold coordinated aluminum is homogeneously distributed throughout the zeolite aggregate, while there are embedded regions rich in 6-fold-coordinated aluminum with sizes extending up to several hundreds of nanometres. These regions are randomly distributed throughout the zeolite particle. In other words, there is no specific 4- and 6-fold aluminum zoning observed within the calcined H-ZSM-5 zeolite aggregate under study.

It should be noted that this result is in apparent contradiction with the earlier reported 2D STXM maps of aluminum for the same sample.[29] However, the reason for the discrepancy observed between the 2D and 3D STXM projections arises from the fact that in a 2D projection the chemical information contained in each pixel refers to the different types of aluminum species present in a column of material. In contrast, in the 3D projection information is contained in several voxels, which can be distinguished from each other. Accordingly, the

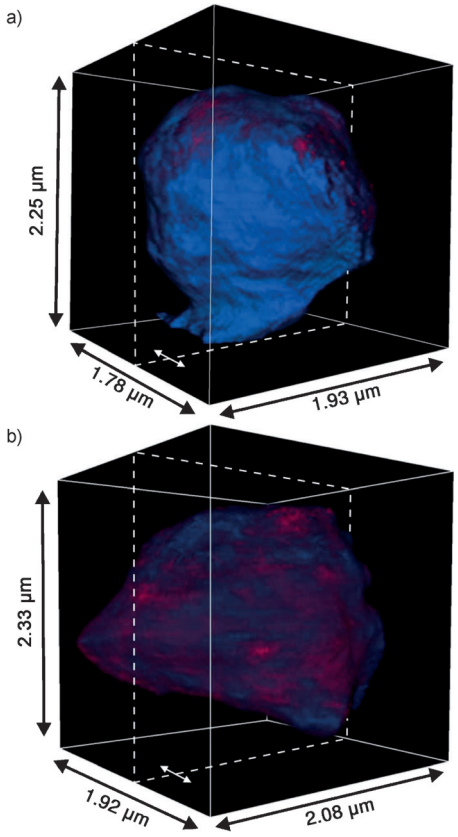

Figure 2. 3D STXM tomographic reconstruction showing the distribution of different aluminum coordination environments for a) sample ZSM-5-C with 4-fold and 6-fold aluminum coloured respectively blue and red; and b) sample ZSM-5-S with 4/5-fold and 6-fold aluminum coloured respectively blue and red.

divergence between the 2D and 3D STXM data indicates that in order to obtain an accurate picture of the distribution of different aluminum coordination within zeolite aggregates nanotomography studies are essential.

In a next step, we have quantified the relative contribution of 4- and 6-fold aluminum species to the overall X-ray absorption within a voxel. Figure 4 shows a histogram of the number of voxels relative to the optical density for 4- and 6-fold coordinated aluminum. Summing up all the voxels measured, comprising the entire zeolite volume, leads to an averaged distribution of both aluminum coordination environments. They correspond to 89% and 11% of 4-fold and 6-fold aluminum, respectively. It is comforting to see that these numbers are very close to those obtained by ^{27}Al MAS NMR measurements on ZSM-5-C.[29] Indeed, the NMR results of 87% for 4-fold aluminum and 13% for 6-fold aluminum are in line with the average numbers from the 3D STXM data analysis. In other words, the nanoscale imaging data are corroborated by independent bulk measurements on the same material.

In contrast, ^{27}Al MAS NMR and STXM measurements reveal that at least two different types of 4-fold aluminum coordination environments as well as 5-fold aluminum species are present after steaming ZSM-5-C (sample ZSM-5-S).[29] As a consequence, the STXM image obtained by subtracting the X-ray absorption at E_1 from that at E_2 is not indicative of a single alumi-

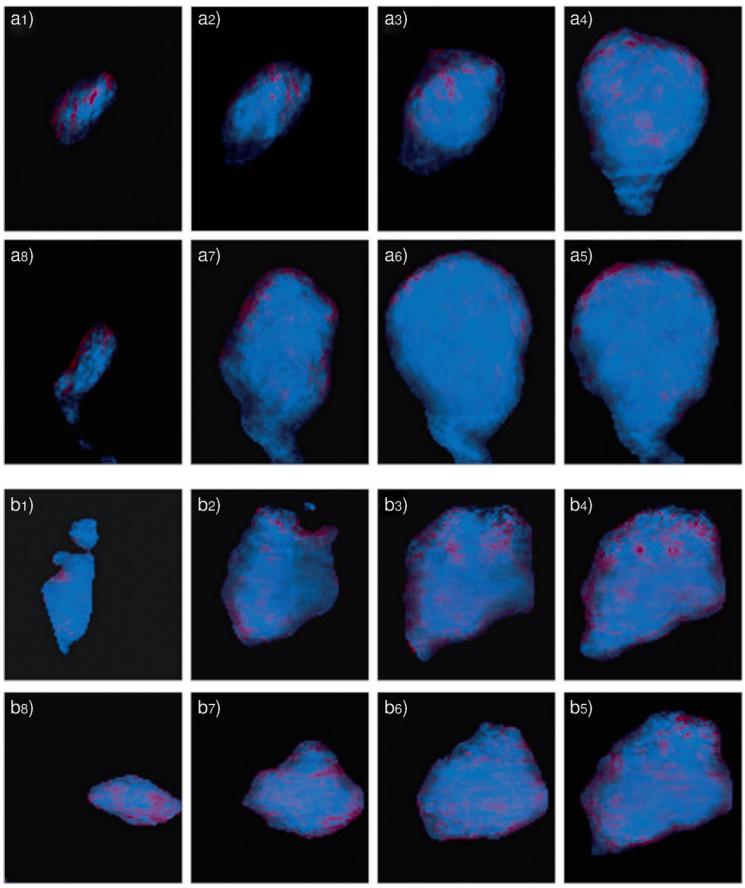

Figure 3. 2D STXM slices obtained from the 3D data cube, shown in Figure 2, for a) an individual ZSM-5-C zeolite aggregate showing 4-fold (blue) and 6-fold (red) aluminum coordination environments in different frames (a1–a8) and b) an individual ZSM-5-S zeolite aggregate showing 4- and 5-fold (blue) and 6-fold (red) aluminum coordination environments in different frames (b1–b8).

num coordination but rather for a mixture of lower aluminum coordination environments (i.e. 4- and 5-fold aluminum). It is noted that, to fully distinguish the individual contributions of the different types of 4-fold and 5-fold aluminum, at least two more 2D STXM projections obtained at different energies are required at every angle. In other words, to unravel the distribution of n different types of aluminum coordination environments $n+1$ 2D STXM projections obtained at different energy values are needed at every angle. Ideally, a series of images over small energy increments, also known as stacks, should be obtained. Nonetheless, the acquisition of a stack with the same settings as those used in the 2D STXM projections collected to obtain the 3D reconstruction will require an acquisition time between 50 and 60 min for every angle. Due to time restrictions during STXM measurements as well as X-ray beam stability issues, we limited our study on ZSM-5-S to the same three energy points E_1, E_2, and E_3, as used for sample ZSM-5-C. Taking into account that the main feature in the aluminum K-edge X-ray absorption spectrum (XAS) of 6-fold coordinated species does not overlap with the edge-jump arising due to the presence of 4-fold and 5-fold aluminum,[31] we will make use of this approach to discuss the relative increase in the amount of 6-fold aluminum with respect to lower aluminum coordination environments upon steaming.

Figure 2b shows the 3D distribution of the amount of 6-fold aluminum relative to that of lower-coordinated aluminum. The corresponding 3D reconstruction for sample ZSM-5-S is further illustrated in Movie SI-2, while Figure 3b shows the 2D STXM slices obtained from the 3D data cube of this movie. These results reveal an overall increase in the aluminum coordination number after hydrothermal treatment. Furthermore, the 3D tomographic reconstruction shows a heterogeneous distribution of 6-fold aluminum species, although no specific aluminum zoning was noted in a steamed H-ZSM-5 zeolite aggregate, at least not within the spatial resolution limitations of our 3D STXM measurements.

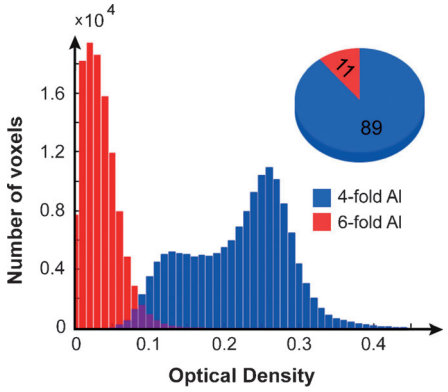

Figure 4. Quantitative analysis of the different aluminum coordination environments within sample ZSM-5-C with 4-fold and 6-fold aluminum coloured respectively blue and red, as obtained from the 3D STXM data cube given in Figure 2.

Summarizing, 3D STXM allows mapping the coordination environment as well as the spatial distribution of aluminum within industrial relevant zeolite catalyst materials. It was found that—at least within the spatial resolution capabilities of the method applied—there is no aluminum zoning within the entire catalyst particle, before as well as after steaming. Nonetheless, the calcined and steamed H-ZSM-5 zeolite aggregates both contain extended regions rich in environments where aluminum is more highly coordinated. Furthermore, it has been possible to quantify the amount of 4- and 6-fold aluminum within the calcined H-ZSM-5 sample. These quantitative numbers for a single zeolite particle are in close agreement with those obtained by bulk analytical tools, such as ^{27}Al MAS NMR. Importantly, this 3D STXM methodology is not limited to aluminum or zeolite materials in general, as different light elements, such as carbon, nitrogen and oxygen, can be measured. Future studies will be directed to in situ measurements able to reveal changes in the state of the catalyst phase and its effect on the nature and distribution of the organic phase present under relevant reaction conditions.

Experimental Section

MFI-Type Zeolite Materials and Steam-Treatment Procedure

Two different zeolite ZSM-5 catalyst powders, namely a calcined (i.e. ZSM-5-C) and a hydrothermally treated sample (i.e. ZSM-5-S) have been investigated. The starting material, with dimensions of approximately 200–800 nm and a Si/Al ratio of 11.5, is a commercial sample provided by Zeolyst (CBV 2314) in their ammonium form. To obtain ZSM-5-C, the starting material was calcined in a static oven (N100 Nabertherm), first preheating the sample at 120 °C (30 min, 2 °C min^{-1}) and then increasing the temperature to 550 °C (360 min, 10 °C min^{-1}). The ZSM-5-S sample was prepared performing a steaming post-treatment on ZSM-5-C. Prior to the hydrothermal treatment, ZSM-5-C was preheated to 120 °C for 30 min in a quartz tubular oven (Thermoline 79300), at a rate of 2 °C min^{-1}. Subsequently, the zeolite sample was heated to 700 °C at a rate of 10 °C min^{-1} and steamed by means of saturation of N_2 flow (180 mL min^{-1}) with water at 100 °C (180 min) to obtain ZSM-5-S. After the hydrothermal treatment the sample was calcined at 550 °C for 360 min in a static oven (N100 Nabertherm).

Acknowledgment

We thank NRSC-C (B.M.W.), NWO-CW Top (B.M.W.) and NWO-CW VICI (F.M.F.d.G.) for financial support.

Keywords: aluminum · heterogeneous catalysis · tomography · X-ray spectroscopy · zeolites

[1] G. Busca, *Chem. Rev.* **2007**, *107*, 5366.
[2] *Introduction to Zeolite Science & Practice* (Eds.: H. van Bekkum, E. M. Flanigen, P. A. Jacobs, J. C. Jansen), Elsevier, Amsterdam, **2001**.
[3] J. Dědeček, D. Kaucky, B. Wichterlova, O. Gonsiorova, *Phys. Chem. Chem. Phys.* **2002**, *4*, 5406.
[4] W. Loewenstein, *Am. Mineral.* **1954**, *39*, 92.
[5] E. G. Derouane, J. P. Gilson, Z. Gabelica, C. Mousty-Desbuquoit, J. Verbist, *J. Catal.* **1981**, *71*, 447.
[6] H. J. Doelle, J. Heering, L. Riekert, L. Marosi, *J. Catal.* **1981**, *71*, 27.
[7] P. Sazama, J. Dědeček, V. Gabova, B. Wichterlova, G. Spoto, S. Bordiga, *J. Catal.* **2008**, *254*, 180.
[8] A. N. Mlinar, P. M. Zimmerman, F. E. Celik, M. Head-Gordon, A. T. Bell, *J. Catal.* **2012**, *288*, 65.
[9] B. M. Weckhuysen, *Angew. Chem.* **2009**, *121*, 5008; *Angew. Chem. Int. Ed.* **2009**, *48*, 4910.
[10] I. L. C. Buurmans, B. M. Weckhuysen, *Nat. Chem.* **2012**, *4*, 873.
[11] A. Abraham, S. H. Lee, C. H. Shin, S. B. Hong, R. Prins, J. A. van Bokhoven, *Phys. Chem. Chem. Phys.* **2004**, *6*, 3031.
[12] T. Chen, A. Men, P. Sun, J. Zhou, Z. Yuan, Z. Guo, J. Wang, D. Ding, H. Li, *Catal. Today* **1996**, *30*, 189.
[13] J. C. Groen, T. Bach, U. Ziese, A. Donk, K. P. de Jong, J. A. Moulijn, J. Pérez-Ramírez, *J. Am. Chem. Soc.* **2005**, *127*, 10792.
[14] J. Dědeček, Z. Sobalík, B. Wichterlová, *Catal. Rev. Sci. Eng.* **2012**, *54*, 135.
[15] S. van Donk, A. H. Janssen, J. H. Bitter, K. P. de Jong, *Catal. Rev. Sci. Eng.* **2003**, *45*, 297.
[16] R. Chal, C. Gerardin, M. Bulut, S. van Donk, *ChemCatChem* **2011**, *3*, 67.
[17] M. Ogura, S. Y. Shinomiya, J. Tateno, Y. Nara, M. Nomura, E. Kikuchi, M. Matsukata, *Appl. Catal. A* **2001**, *219*, 33.
[18] S. L. Suib, G. D. Stucky, *J. Catal.* **1980**, *65*, 174.
[19] R. von Ballmoos, W. M. Meier, *Nature* **1981**, *289*, 782.
[20] R. Althoff, B. Sellegreen, B. Zibrowius, K. Unger, F. Schuth, in *Synthesis of Porous Materials: Zeolites, Clays and Nanostructures* (Eds.: M. L. Ocelli, H. Kessler), Marcel Dekker, New York, **1997**, pp. 139.
[21] J. C. Lin, K. J. J. Chao, *J. Chem. Soc. Faraday Trans. 1* **1986**, *82*, 2645.
[22] L. Karwacki, M. H. F. Kox, D. A. M. de Winter, M. R. Drury, J. D. Meeldijk, E. Stavitski, W. Schmidt, M. Mertens, P. Cubillas, N. John, A. Chan, N. Kahn, S. R. Bare, M. Anderson, J. Kornatowski, B. M. Weckhuysen, *Nat. Mater.* **2009**, *8*, 959.
[23] H. Kessler, J. Patarin, C. Schott-Darie, *Stud. Surf. Sci. Catal.* **1994**, *85*, 75.
[24] G. Debras, A. Gourgue, J. B. Nagy, *Zeolites* **1985**, *5*, 369.
[25] K. J. Chao, J. Y. Chern, *Zeolites* **1988**, *8*, 82.
[26] R. M. Dessau, E. W. Valyocsik, N. H. Goeke, *Zeolites* **1992**, *12*, 776.
[27] M. M. van Schooneveld, J. Hilhorst, A. V. Petukhov, T. Tyliszczak, J. Wang, B. M. Weckhuysen, F. M. F. de Groot, E. de Smit, *Small* **2011**, *7*, 804.
[28] J. Hilhorst, M. M. van Schooneveld, J. Wang, E. de Smit, T. Tyliszczak, J. Raabe, A. P. Hitchcock, M. Obst, F. M. F. de Groot, A. V. Petukhov, *Langmuir* **2012**, *28*, 3614.
[29] L. R. Aramburo, E. d. Smit, B. Arstad, M. M. v. Schooneveld, L. Sommer, A. Juhin, T. Yokosawa, H. W. Zandbergen, U. Olsbye, F. M. F. de Groot, B. M. Weckhuysen, *Angew. Chem. Int. Ed.* **2012**, *51*, 3616.
[30] A. L. D. Kilcoyne, T. Tyliszczak, W. F. Steele, S. Fakra, P. Hitchcock, K. Franck, E. Anderson, B. Harteneck, E. G. Rightor, G. E. Mitchell, A. P. Hitchcock, L. Yang, T. Warwick, H. Ade, *J. Synchrotron Radiat.* **2003**, *10*, 125.
[31] P. Ildefonse, D. Cabaret, P. Sainctavit, G. Calas, A. M. Flank, P. Lagarde, *Phys. Chem. Miner.* **1998**, *25*, 112.

Received: December 5, 2012
Published online on January 4, 2013